

# GALEX Observations of CS and OH Emission in Comet 9P/Tempel 1 During Deep Impact<sup>1</sup>

Paul D. Feldman<sup>2</sup>, Stephan R. McCandliss<sup>2</sup>, Jeffrey P. Morgenthaler<sup>3</sup>,  
Carey M. Lisse<sup>4</sup>, Harold A. Weaver<sup>4</sup>, and Michael F. A'Hearn<sup>5</sup>

pdf@pha.jhu.edu

## ABSTRACT

*GALEX* observations of comet 9P/Tempel 1 using the near ultraviolet (NUV) objective grism were made before, during and after the Deep Impact event that occurred on 2005 July 4 at 05:52:03 UT when a 370 kg NASA spacecraft was maneuvered into the path of the comet. The NUV channel provides usable spectral information in a bandpass covering 2000 – 3400 Å with a point source spectral resolving power of  $R \approx 100$ . The primary spectral features in this range include solar continuum scattered from cometary dust and emissions from OH and CS molecular bands centered near 3085 and 2575 Å, respectively. In particular, we report the only cometary CS emission detected during this event. The observations allow the evolution of these spectral features to be tracked over the period of the encounter. In general, the NUV emissions observed from Tempel 1 are much fainter than those that have been observed by *GALEX* from other comets. However, it is possible to derive production rates for the parent molecules of the species detected by *GALEX* in Tempel 1 and to determine the number of these molecules liberated by the impact. The derived quiescent production rates are  $Q(\text{H}_2\text{O}) = 6.4 \times 10^{27}$  molecules  $\text{s}^{-1}$  and  $Q(\text{CS}_2) = 6.7 \times 10^{24}$  molecules  $\text{s}^{-1}$ , while the impact produced an additional  $1.6 \times 10^{32}$  H<sub>2</sub>O molecules and  $1.3 \times 10^{29}$  CS<sub>2</sub> molecules, a similar ratio as in quiescent outgassing.

*Subject headings:* comets: individual (9P/Tempel 1) — ultraviolet: solar system

---

<sup>1</sup>Based on observations made with the NASA *Galaxy Evolution Explorer*. *GALEX* is operated for NASA by the California Institute of Technology under NASA contract NAS5-98034

<sup>2</sup>Department of Physics and Astronomy, The Johns Hopkins University, Baltimore, MD 21218-2695

<sup>3</sup>Planetary Science Institute, 1700 E. Fort Lowell, Suite 106, Tucson, AZ 85719-2395

<sup>4</sup>Johns Hopkins University Applied Physics Laboratory, Space Department, 11100 Johns Hopkins Road, Laurel, MD 20723-6099

<sup>5</sup>Astronomy Department, University of Maryland, College Park, MD 20742-2421

## 1. Introduction

On 2005 July 4 at 05:52:03 UT (as seen from Earth) a 370 kg NASA spacecraft was maneuvered into the path of comet 9P/Tempel 1 (A'Hearn et al. 2005). The results of the impact were recorded by a host of ground and space based observatories with wavelength coverage spanning the sub-mm to the ultraviolet (Meech et al. 2005). Here we report on the results of low resolution slitless spectroscopy acquired with the *Galaxy Evolution Explorer* (*GALEX*) in the near ultraviolet NUV channel 2 days before, immediately following, and 1 day after the impact event. The primary spectral features in this range include a solar continuum scattered from cometary dust and emissions from OH and CS molecular bands centered near 3085 and 2575 Å, respectively.

## 2. Observations

*GALEX* (*Galaxy Evolution Explorer*) is a NASA Small Explorer whose primary mission is to map the history of star formation using two modes: two-band photometry (FUV, 1350–1750 Å; NUV, 1750–3100 Å) and integrated field grism spectroscopy with 10–20 Å spectral resolution. Because of its large field-of-view,  $1^{\circ}2$ , *GALEX* is also well suited to cometary coma studies as demonstrated by the 2005 March observations of C/2004 Q2 Machholz (Morgenthaler et al. 2006). It has a limiting spatial resolution in the NUV channel of  $\approx 5''$  sampled with  $1''.5$  pixels. For *Deep Impact* only NUV data was obtained as the FUV side was not operating at time of the event. In all there were 7 contiguous pre-impact orbits devoted to grism observations, with  $\approx 900$  s visibility per orbit. Two orbits of direct imaging were taken before and after the grism orbits. For the impact event there were 6 orbits of grism observations beginning a few minutes after impact, with direct imaging before (1 orbit) and after (2 orbits). One day post-impact there were 4 orbits of grism observations with one direct imaging orbit before the grism observations. A log of the spectroscopic observations is given in Table 1. Here we concentrate on the results derived from the low resolution slitless spectroscopy in the NUV channel.

At the time of impact comet 9P/Tempel 1 was at a distance of  $r = 1.51$  AU from the Sun and  $\Delta = 0.89$  AU from the Earth. A  $1''.5$  pixel subtended 975 km at the comet. Emission from OH, CS, and solar scattered light were detected prior to impact. Just after impact the brightness and spatial extent of these emissions increased with time. The following day saw the return of these emissions to near the pre-impact levels.

## 2.1. Data Extraction

The *GALEX* project supplied a time-tagged photon list of the observations with photon coordinates referenced to RA and DEC (J2000). The project also supplied the output of Emmanuel Bertin's SExtractor program run on the direct-mode (imaging) observations centered on the same fields. SExtractor provides accurate astrometry for sources found in the direct images. We converted these positions into rectangular strips using the *GALEX* dispersion relation for box length and the magnitude estimates from SExtractor for box widths in order to mask sources in the grism images. All of our astrometric corrections were done on a spherical projection with the IDLASTRO routines. Co-alignment between the strips and the grism images of the stars across the entire image confirmed the accuracy of these calculations. We used the JPL HORIZONS ephemeris generator with *GALEX* as the observatory ("@galex") to calculate the astrometrically correct ephemeris for comet Tempel 1. The ephemeris was used to reconstruct the comet image from the photon list in the reference frame of the comet. Counts and exposure times were accumulated into separate images and the source mask and flat field (supplied by the *GALEX* project) were applied every time the stars moved by one pixel relative to the comet. As a result, emission from well-characterized sources was effectively erased and very little exposure time was lost. The final rate images, constructed by dividing the total count images by the total exposure time images for the corresponding observations, were used in the analysis of the temporal evolution of the coma following the impact.

Because of the low total counts in each individual grism image, individual exposures were summed to produce a composite image from each day of the program. In this case the source mask was not applied and the stellar spectra appear as multiple images separated by the comet's motion between *GALEX* orbits. An example is shown in Figure 1 for the sum of the six grism images obtained following the impact event. Note that the stellar images (each corresponding to a different orbit) are broadened by their apparent relative motion nearly normal to the dispersion direction during the exposure.

## 3. Analysis

Analysis of the spectrum is begun with the composite images (such as in Figure 1) corresponding to the *GALEX* orbits from the three dates of observation. The spectra are extracted over 13 rows of the rotated image array, corresponding to an effective slit height of  $19.''5$  to ensure that only pixels with statistically significant counts are included in the aperture photometry. The detector background is evaluated over the same rows in the spectral range 1700 to 2000 Å where the NUV throughput for a solar-like spectrum is effectively zero. This background is subject to variation due to the presence of faint stars or galaxies in the field. The three composite spectra, after

subtraction of background, are shown in the top panels of Figure 2. The extraction of the discrete emissions from CS and OH is complicated by the blended continuous solar spectrum produced by the scattering of sunlight by cometary dust grains in the coma. An additional complication arises from the different spatial distributions of the dust and gas components that result from the quiescent outflow and the subsequent time evolution of these distributions after the impact, as the spatial variation is superimposed on the actual spectrum in the dispersion direction.

Between 2000 and 3400 Å the solar spectrum rises steeply and at the long wavelength end can contribute to the extended OH(0,0) band near 3085 Å. Since the effective area,  $A_{eff}$ , supplied by the *GALEX* project did not extend beyond 3100 Å, we identified a field F8 V star and an *IUE* calibration standard to extend  $A_{eff}$  to 3400 Å. A model of the dust scattered solar continuum is required to account for the contamination of the OH(0,0) and CS(0,0) bands. We used a solar spectrum from UARS/Solstice, described by Woods et al. (1996), multiplied by this  $A_{eff}$ , and convolved with a superposition of  $\sim 80$  Å and  $\sim 250$  Å Gaussian instrument functions to simulate the radially outflowing dust in the dispersion direction, in order to generate a template for the solar scattered light. This template, normalized to regions of the spectrum where strong molecular emission is absent, and reddened by 4% per 100 Å (Feldman & A'Hearn 1985), is also shown in the figure. The difference between the observed spectra and the template is shown in the lower panels of the same figure.

The three identified emission features are the CS(0,0) band at 2576 Å, and the OH(1,0) and (0,0) bands at 2820 and 3085 Å, respectively. For near zero heliocentric velocity, the ratio of fluorescence efficiencies of the OH(1,0) and (0,0) bands is 0.10 (Schleicher & A'Hearn 1988), but the *GALEX* effective area is 4.2 times higher at 2820 Å than at 3085 Å, so the (1,0) band should give a count rate  $\sim 0.4$  that of the (0,0) band. This is consistent with the lower panels of Figure 2, and serves to validate the continuum subtraction. In principle, we could use the template scaling factor to derive the temporal variation of the dust ejected by the impact, but this is much better done with visible observations from the ground or from space (e.g., Schleicher et al. 2006; Feldman et al. 2007) because of uncertainties in the background subtraction.

*GALEX* observations began only a few minutes after the impact and grism spectra were recorded on six successive orbits, or for about 8.5 hours following the impact. The temporal evolution of the CS and OH emissions can be seen in the individual spectra shown in Figure 3. To construct a light curve, we used a rectangular aperture wide enough to capture almost all of the band emission, keeping the aperture height at 19.''5, as above. For CS, the width was 22.''5, corresponding to a spectral bandwidth of 100 Å, while for OH the width was 46.''5, or  $\sim 200$  Å. The projected sizes on the sky are  $12,600 \times 14,500$  km and  $12,600 \times 30,000$  km, respectively for CS and OH. Similar photometry was performed on the pre- and post-impact data sets, and the results are shown in Figure 4, in which the plotted times are the mid-points of the exposure. The

observations beginning about 24 hours after impact show the gaseous emissions returning to near quiescent levels.

#### 4. Discussion

The quiescent production rates were determined using the vectorial model of Festou (1981). The parent lifetimes at 1 AU were 71,000 s for H<sub>2</sub>O, with 85% of the dissociations producing OH (Budzien et al. 1994), and 1,000 s for CS<sub>2</sub> (Feldman et al. 1999). The lifetimes of OH and CS were taken to be 140,000 s and 100,000 s, respectively, but are not critical for the aperture size used. The parent outflow velocity in the model is  $0.85r^{-1/2}$  km s<sup>-1</sup>, while the daughters are given 1.05 and 0.90 km s<sup>-1</sup>, for OH and CS, respectively. The fluorescence efficiencies at 1 AU are  $2.3 \times 10^{-4}$  and  $5.4 \times 10^{-4}$  photons s<sup>-1</sup> molecule<sup>-1</sup> for the OH(0,0) band (Schleicher & A'Hearn 1988) and the CS(0,0) band (R. Yelle, private communication), respectively. The derived production rates are given in Table 2, together with other recently reported values. Our value for the water production rate fits squarely within the range reported previously. We also note that the CS<sub>2</sub>/H<sub>2</sub>O production rate ratio,  $9.5 \times 10^{-4}$ , is typical of values found from *IUE* observations of comets (Meier & A'Hearn 1997).

The linear increase with time following impact in the number of dissociation products in the aperture can be modeled, using known photochemical rates (Feldman et al. 2004), to determine the abundance of the parent molecular species produced in the collision. This approach was used by Küppers et al. (2005) for the analysis of wide-field camera images of OH emission. However, for our aperture height of 12,600 km, molecules flowing radially outward at a mean velocity of 0.5 km s<sup>-1</sup> will begin to exit the aperture 3.5 hours after impact. This problem was considered by Manfroid et al. (2007), and we adopt their formalism. In addition to the parent and daughter species, whose photochemical lifetimes are given above, Manfroid et al. also include a “grandparent” molecule to account for gas excavation over an extended period (several minutes) or evaporation from excavated icy grains. The “lifetime” of the grandparent is an adjustable parameter.

The model results are shown with the data in Figure 4. For a baseline, we adopt the mean value of pre-impact count rates, which correspond to an observation almost exactly one rotation period ( $\sim 41$  hours) earlier. The CS light curve is well fit by a mean velocity of 0.4 km s<sup>-1</sup> and a velocity dispersion of 0.1 km s<sup>-1</sup>, similar to the values derived by Manfroid et al. for various radicals, and a “grandparent” lifetime of 2000 s. For OH, models with 0.4 km s<sup>-1</sup> and 0.5 km s<sup>-1</sup> are shown in the figure. What matters most in deriving the number of parent molecules produced is the linear increase immediately following the impact before any of the dissociation products has left the field-of-view. We note that Feldman et al. (2006) found a maximum velocity of CO produced by the impact to be 0.7 km s<sup>-1</sup>.

The total number of molecules found is  $\sim 1.3 \times 10^{29}$  molecules of  $\text{CS}_2$  and  $\sim 1.6 \times 10^{32}$  molecules of  $\text{H}_2\text{O}$  (corresponding to  $\sim 1.6 \times 10^4$  kg and  $\sim 4.6 \times 10^6$  kg, respectively). The  $\text{CS}_2/\text{H}_2\text{O}$  ratio is  $8.0 \times 10^{-4}$ , comparable to the quiescent value within the given uncertainties. A comparison with other reported values is given in Table 3, and shows generally good agreement. Our numbers are lower, by 25% for  $\text{H}_2\text{O}$  and a factor of 3 for  $\text{CS}_2$ , than those presented in 2006 in a preliminary report on these results (Feldman 2009). The spectral images used in that analysis did not have the comet's motion removed and so a large extraction box was used to ensure that all of the cometary photons were counted. This made it difficult to properly subtract the dust continuum, which is more important for isolating the CS emission than it is for the OH emission. We note that the only uncertainties in the derivation of the total number of molecules produced (other than due to photon statistics and absolute calibration) are those in the photodissociation lifetimes and fluorescence efficiencies, which are known at the 10% level. The combined uncertainties are  $\approx 20\%$ .

After 25 hours all gas and dust emissions within the summation aperture have returned to nearly quiescent values. However, as the lower right panel of Fig. 2 shows, the OH bands one day after impact appear much broader in wavelength than prior to impact, likely due to outflow along the dispersion direction. This is not surprising as at 1.5 AU the photodissociation lifetimes of  $\text{H}_2\text{O}$  and OH are 2 and 3 days, respectively.

Two other orbiting spacecraft made NUV observations of the *Deep Impact* event: both are X-ray observatories with UV/optical imagers that were used with wide-band NUV filters. The filter passband of the *Swift* imager included both the CS and OH bands in addition to dust continuum (Mason et al. 2007) but the photometric images are dominated by the OH emission. The number of water molecules produced by the impact derived from their photometry (see Table 3) is in excellent agreement with our result. The *XMM-Newton* observatory imager had two NUV filters, one of which included only CS emission while the other included both CS and OH (Schulz et al. 2006). The light curves derived from both filters show behavior similar to that of the two light curves in Figure 4. Schulz et al. attribute the difference in shape of the light curves to the presence of small “icy grains” in the ejecta. However, as the *GALEX* spectra of Figure 2 demonstrate, their data can be reasonably accounted for by CS emission.

## 5. Conclusion

*GALEX* observations of comet 9P/Tempel 1 at the time of *Deep Impact* provide a unique measurement of the CS parent produced by the excavation of cometary material, and as with other daughter molecules, appears to have the same abundance relative to  $\text{H}_2\text{O}$  as in quiescent outgassing of the comet. Our derived value for the amount of  $\text{H}_2\text{O}$  excavated is in excellent agreement with

the results of several other investigations. This reinforces the idea that nearly all the volatile species are uniformly mixed with the water ice from the near-surface layer at which sublimation normally occurs to the tens of meters to which *Deep Impact* excavated material. This lack of differentiation from near-surface to tens of meters implies either that the surface erodes (due to hydrodynamic drag on the dust by the gas) at about the same rate as the differentiation front proceeds deeper or that the differentiation has reached depths of many tens of meters while somehow still leaving the same relative fraction of all the volatiles throughout the upper tens of meters (A'Hearn 2008). Notwithstanding the relative faintness of the comet, the *GALEX* results demonstrate the unique capability of wide-field imaging spectroscopy of comets in the ultraviolet at wavelengths below the atmospheric cutoff.

We thank the *GALEX* project, and Karl Forster in particular, for their efforts in planning and executing these observations. We would like to acknowledge Tim Conrow and the *GALEX* pipeline processing team for helping us to fully utilize the moving target capability of *GALEX*, Jon Giorgini and the JPL HORIZONS team for calculating high precision comet ephemerides from the perspective of *GALEX*, and Wayne Landsman and the many contributors to the IDLASTRO library. This work was supported by the *GALEX* Guest Investigator program under NASA grant NNC06GD35G to the Johns Hopkins University.

*Facilities:* GALEX.

## REFERENCES

- A'Hearn, M. F. 2008, *Space Science Reviews*, 138, 237
- A'Hearn, M. F., et al. 2005, *Science*, 310, 258
- Bensch, F., Melnick, G. J., Neufeld, D. A., Harwit, M., Snell, R. L., Patten, B. M., & Tolls, V. 2007, *Icarus*, 191, 267
- Biver, N., et al. 2007, *Icarus*, 187, 253
- Budzien, S. A., Festou, M. C., & Feldman, P. D. 1994, *Icarus*, 107, 164
- DiSanti, M. A., Villanueva, G. L., Bonev, B. P., Magee-Sauer, K., Lyke, J. E., & Mumma, M. J. 2007, *Icarus*, 187, 240
- Feldman, P. D. 2009, *Deep Impact as a World Observatory Event: Synergies in Space, Time, and Wavelength*, ed. H. U. Käufel & C. Sterken, 227

- Feldman, P. D., & A'Hearn, M. F. 1985, in NATO ASIC Proc. 156: Ices in the Solar System, ed. J. Klinger, D. Benest, A. Dollfus, & R. Smoluchowski, 453
- Feldman, P. D., Cochran, A. L., & Combi, M. R. 2004, in Comets II, ed. M. C. Festou, H. A. Weaver, & H. U. Keller (Tucson: Univ. of Arizona), 425
- Feldman, P. D., Lupu, R. E., McCandliss, S. R., Weaver, H. A., A'Hearn, M. F., Belton, M. J. S., & Meech, K. J. 2006, *ApJ*, 647, L61
- Feldman, P. D., McCandliss, S. R., Route, M., Weaver, H. A., A'Hearn, M. F., Belton, M. J. S., & Meech, K. J. 2007, *Icarus*, 187, 113
- Feldman, P. D., Weaver, H. A., A'Hearn, M. F., Festou, M. C., McPhate, J. B., & Tozzi, G.-P. 1999, *BAAS*, 31, 1127
- Festou, M. C. 1981, *A&A*, 95, 69
- Keller, H. U., et al. 2007, *Icarus*, 187, 87
- Küppers, M., et al. 2005, *Nature*, 437, 987
- Manfroid, J., et al. 2007, *Icarus*, 191, 348
- Mason, K. O., et al. 2007, *Icarus*, 187, 123
- Meech, K. J., et al. 2005, *Science*, 310, 265
- Meier, R., & A'Hearn, M. F. 1997, *Icarus*, 125, 164
- Morghenthaler, J. P., Harris, W. M., Combi, M. R., Feldman, P. D., & Weaver, H. A. 2006, *BAAS*, 38, 935
- Schleicher, D. G., & A'Hearn, M. F. 1988, *ApJ*, 331, 1058
- Schleicher, D. G., Barnes, K. L., & Baugh, N. F. 2006, *AJ*, 131, 1130
- Schulz, R., Owens, A., Rodriguez-Pascual, P. M., Lumb, D., Erd, C., & Stüwe, J. A. 2006, *A&A*, 448, L53
- Woods, T. N., et al. 1996, *J. Geophys. Res.*, 101, 9541

Table 1. *GALEX* Grism Observation Log of Comet 9P/Tempel 1.

FILENAME	EXPTIME (s)	DATE-OBS	TIME-OBS
GI1_024001_DEEP_IMPACT_PRE_0001-ng-int.fits	820.0	2005-07-02	06:22:17
GI1_024001_DEEP_IMPACT_PRE_0002-ng-int.fits	940.0	2005-07-02	08:00:53
GI1_024001_DEEP_IMPACT_PRE_0003-ng-int.fits	940.0	2005-07-02	09:39:29
GI1_024001_DEEP_IMPACT_PRE_0004-ng-int.fits	960.0	2005-07-02	11:18:04
GI1_024001_DEEP_IMPACT_PRE_0005-ng-int.fits	940.0	2005-07-02	12:56:41
GI1_024001_DEEP_IMPACT_PRE_0006-ng-int.fits	940.0	2005-07-02	14:35:17
GI1_024001_DEEP_IMPACT_PRE_0007-ng-int.fits	940.0	2005-07-02	16:13:53
GI1_024002_DEEP_IMPACT_0001-ng-int.fits	759.0	2005-07-04	06:01:47
GI1_024002_DEEP_IMPACT_0002-ng-int.fits	959.0	2005-07-04	07:40:23
GI1_024002_DEEP_IMPACT_0003-ng-int.fits	939.0	2005-07-04	09:18:59
GI1_024002_DEEP_IMPACT_0004-ng-int.fits	938.1	2005-07-04	10:57:36
GI1_024002_DEEP_IMPACT_0005-ng-int.fits	940.0	2005-07-04	12:36:11
GI1_024002_DEEP_IMPACT_0006-ng-int.fits	939.0	2005-07-04	14:14:48
GI1_024003_DEEP_IMPACT_POST_0001-ng-int.fits	299.0	2005-07-05	05:05:56
GI1_024003_DEEP_IMPACT_POST_0002-ng-int.fits	919.0	2005-07-05	06:40:52
GI1_024003_DEEP_IMPACT_POST_0003-ng-int.fits	931.2	2005-07-05	08:19:29
GI1_024003_DEEP_IMPACT_POST_0004-ng-int.fits	939.0	2005-07-05	09:58:05

Table 2: Quiescent production rates (in molecules  $s^{-1}$ ) in 9P/Tempel 1.

Reference	Observation	H <sub>2</sub> O ( $\times 10^{27}$ )	CS <sub>2</sub> ( $\times 10^{24}$ )
This paper	OH/CS - UV ( <i>GALEX</i> )	6.4	6.7
Keller et al. (2007)	OH - UV ( <i>Rosetta</i> )	4.2–4.4	
Schleicher et al. (2006)	OH - UV (ground)	6	
DiSanti et al. (2007)	H <sub>2</sub> O - IR	9.4	
Bensch et al. (2007)	H <sub>2</sub> O - sub-mm ( <i>SWAS</i> )	5.2	
Biver et al. (2007)	H <sub>2</sub> O/CS - sub-mm ( <i>ODIN</i> )	9.1	< 19.7 <sup>a</sup>

---

<sup>a</sup>Post-impact on 6 July.

Table 3: Total number of water molecules produced by the impact.

Reference	Observation	H <sub>2</sub> O ( $\times 10^{32}$ )
This paper	OH - UV ( <i>GALEX</i> )	1.6
Mason et al. (2007)	OH - UV ( <i>SWIFT</i> )	$1.4 \pm 0.2$
Keller et al. (2007)	OH - UV ( <i>Rosetta</i> )	1.5–3.0
Bensch et al. (2007)	H <sub>2</sub> O - sub-mm ( <i>SWAS</i> )	< 5.9 (3- $\sigma$ )
Biver et al. (2007)	H <sub>2</sub> O - sub-mm ( <i>ODIN</i> )	$1.7 \pm 0.7$

### FIGURE CAPTIONS

Fig. 1.— The central  $12'.8 \times 12'.8$  of the composite *GALEX* NUV grism image taken in the 8.5 h following the *Deep Impact* encounter with comet 9P/Tempel 1. The motion of the comet is nearly perpendicular to the dispersion as can be seen from the multiple, wide stellar spectra. The image has been rotated  $48^\circ$  east from north. Nearly point-like CS and continuum emission together with diffuse OH emission at  $3085 \text{ \AA}$  can be seen in the spectrum.

Fig. 2.— Composite *GALEX* NUV spectra of comet 9P/Tempel 1 for each of the three days of observation as listed in Table 1. Background counts have been subtracted. The top panels show the fit to solar scattered light in red, while the lower panels show the spectrum with the solar light subtracted. The peak wavelengths of the CS (0,0) and OH (1,0) and (0,0) bands are indicated. Note, in the post-impact spectra, the broadening of the OH emissions due to outflow along the dispersion direction.

Fig. 3.— Same as the top panels in Figure 2 for the six consecutive *GALEX* orbits taken immediately following the impact, showing the temporal evolution of the emissions.

Fig. 4.— Temporal evolution of the CS (top) and OH (bottom) emissions. The left panels show the count rates roughly one comet rotation ( $\sim 41$  hours) prior to the impact. Model fits to the aperture photometry are shown for velocities of  $0.4 \text{ km s}^{-1}$  (dashed line) and  $0.5 \text{ km s}^{-1}$  (dotted line).

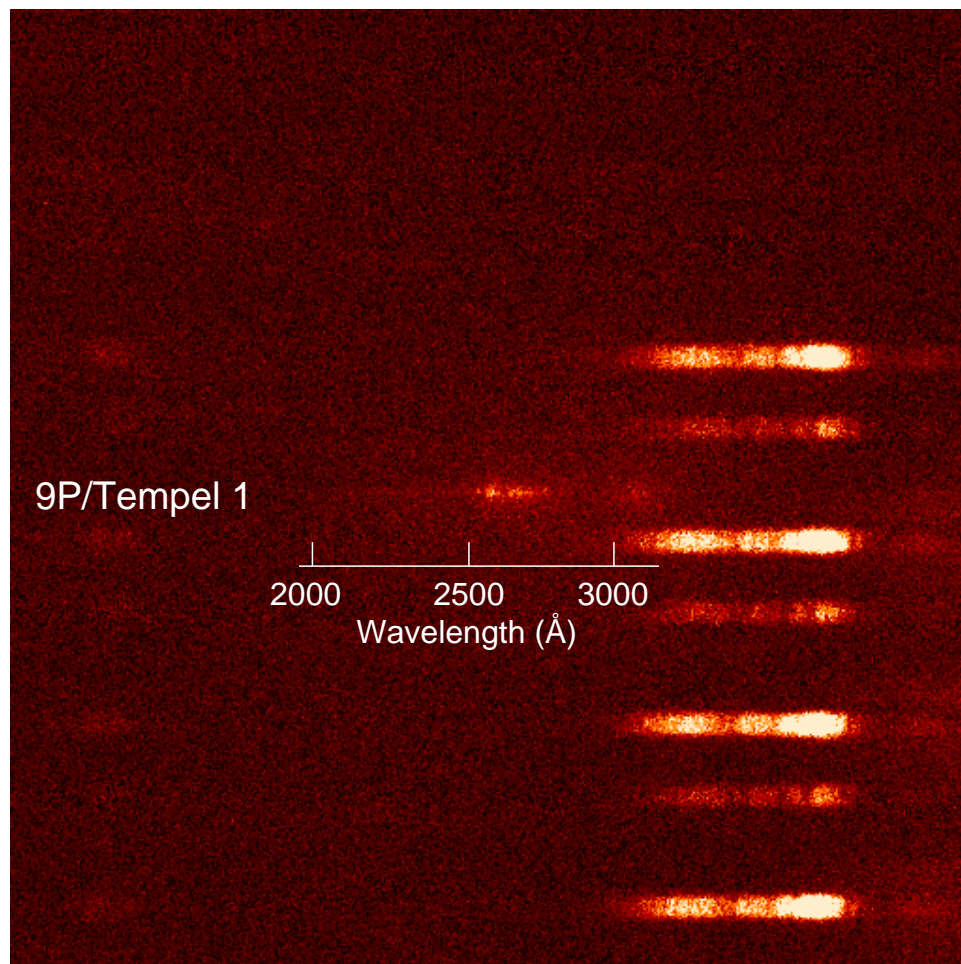


Fig. 1.— The central  $12'.8 \times 12'.8$  of the composite *GALEX* NUV grism image taken in the 8.5 h following the *Deep Impact* encounter with comet 9P/Tempel 1. The motion of the comet is nearly perpendicular to the dispersion as can be seen from the multiple, wide stellar spectra. The image has been rotated  $48^\circ$  east from north. Nearly point-like CS and continuum emission together with diffuse OH emission at  $3085 \text{ \AA}$  can be seen in the spectrum.

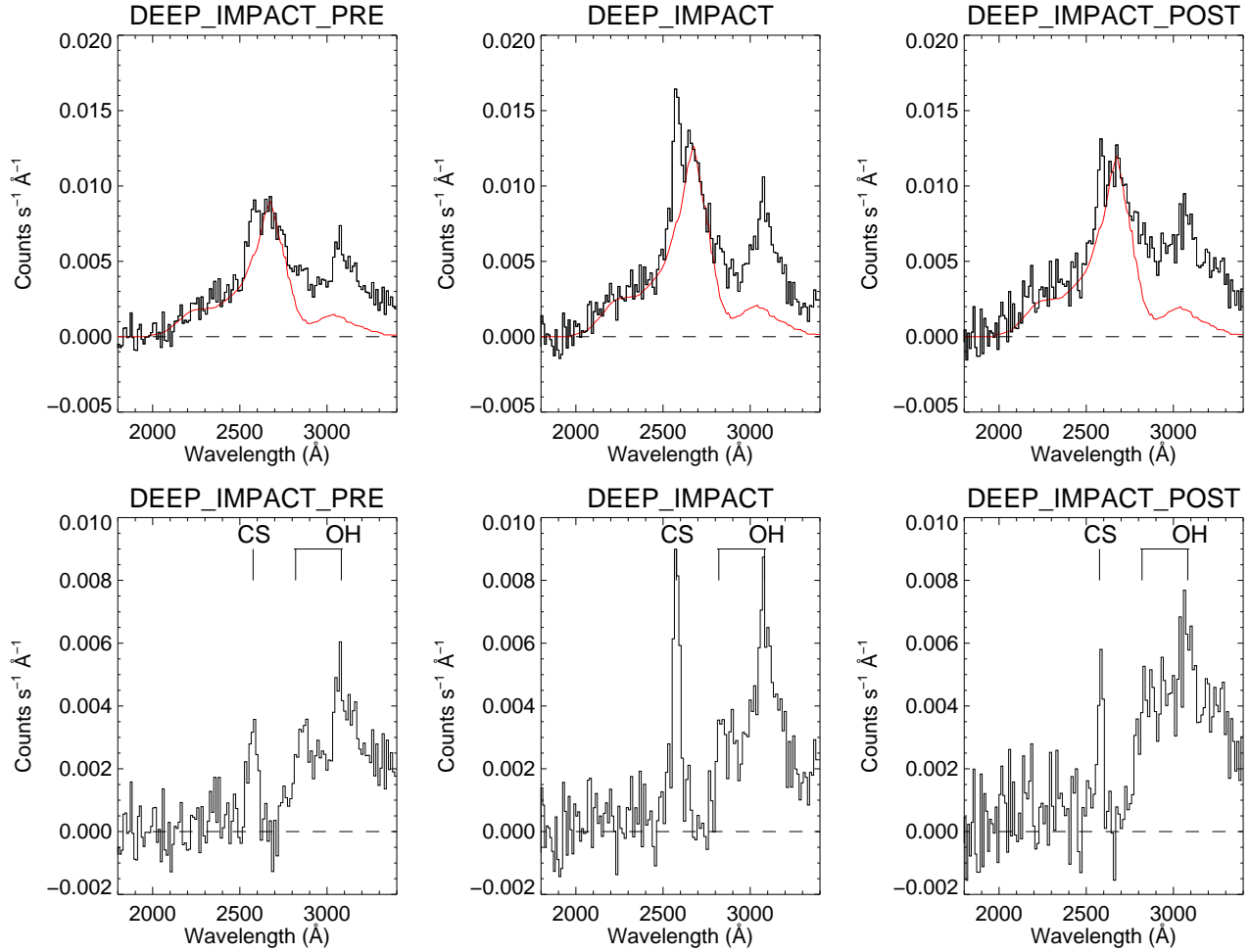


Fig. 2.— Composite *GALEX* NUV spectra of comet 9P/Tempel 1 for each of the three days of observation as listed in Table 1. Background counts have been subtracted. The top panels show the fit to solar scattered light in red, while the lower panels show the spectrum with the solar light subtracted. The peak wavelengths of the CS (0,0) and OH (1,0) and (0,0) bands are indicated. Note, in the post-impact spectra, the broadening of the OH emissions due to outflow along the dispersion direction.

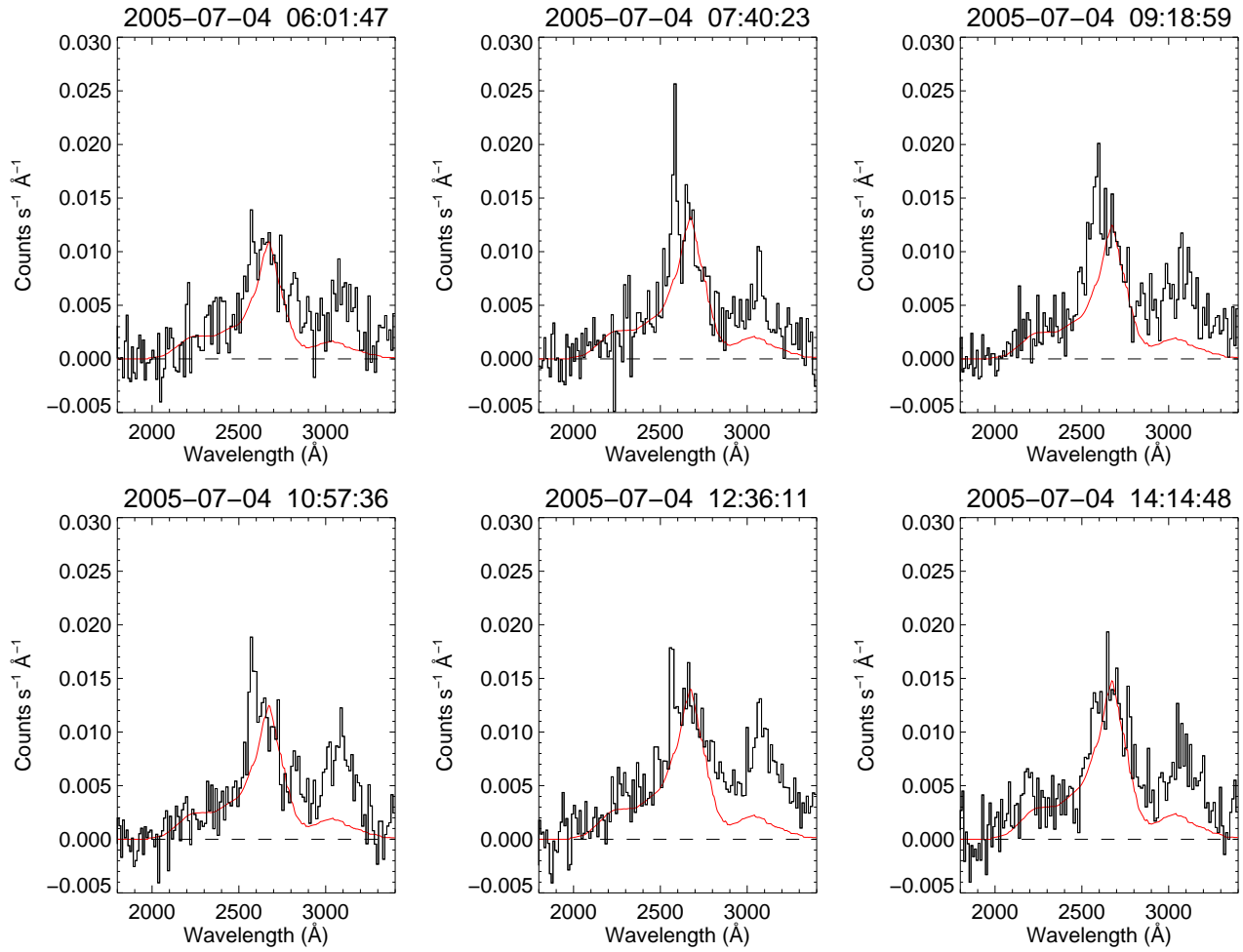


Fig. 3.— Same as the top panels in Figure 2 for the six consecutive *GALEX* orbits taken immediately following the impact, showing the temporal evolution of the emissions.

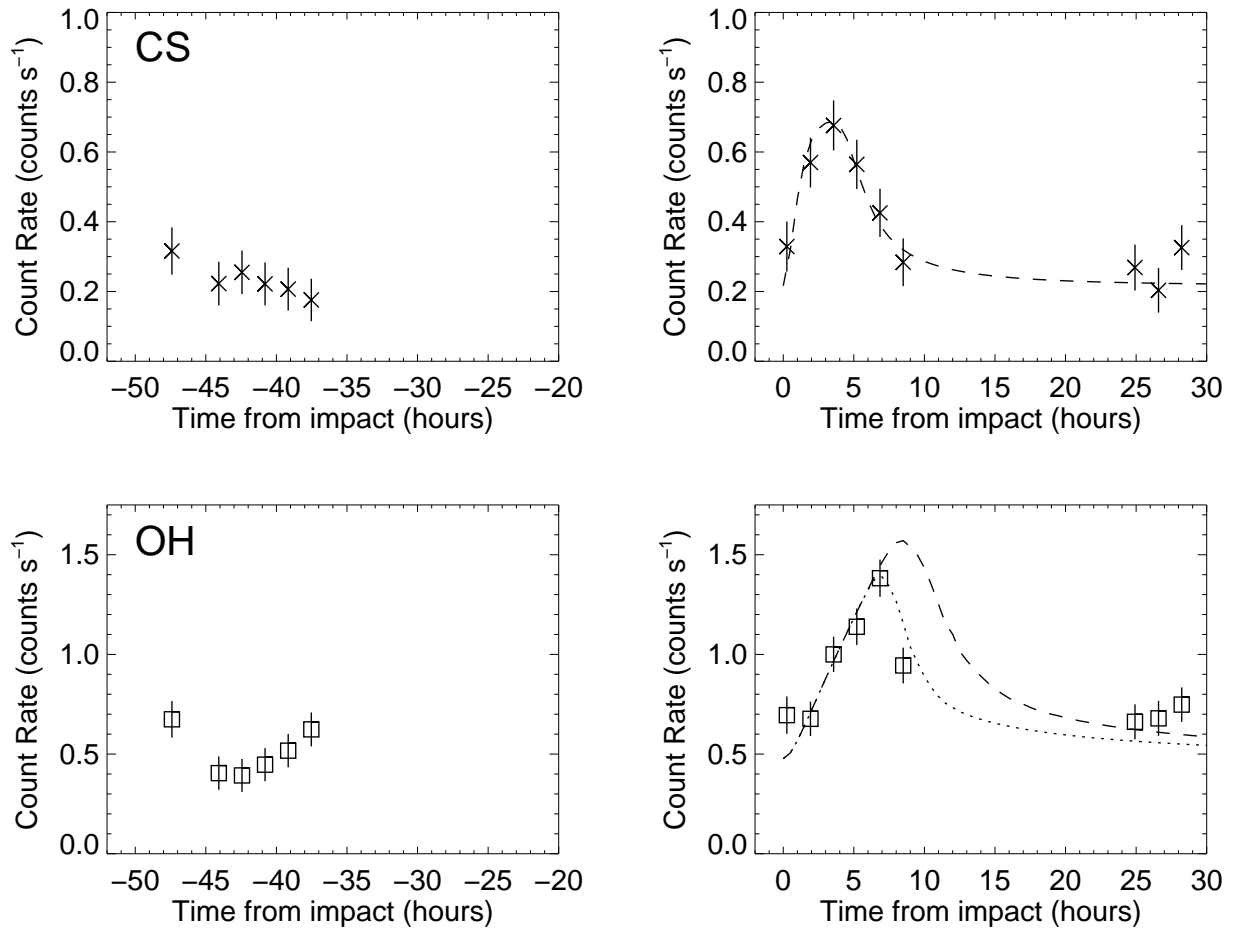


Fig. 4.— Temporal evolution of the CS (top) and OH (bottom) emissions. The left panels show the count rates roughly one comet rotation ( $\sim 41$  hours) prior to the impact. Model fits to the aperture photometry are shown for velocities of  $0.4 \text{ km s}^{-1}$  (dashed line) and  $0.5 \text{ km s}^{-1}$  (dotted line).